Chapter 9
Mechanistic Aspects of Fracture I—Brittle Fracture Models

The fracture of materials is a mechanistic event, and the mechanistic scheme and describing the function of hydrogen in the fracture process are required. In the latter half of the twentieth century, recognition of the involvement of hydrogen in the failure of structural steel components, like delayed cracking and degradation in mechanical testing, overlapped with developing fracture mechanics that addressed brittle fracture.

Hydrogen-related fracture of high-strength steel is mostly brittle-like without substantial apparent plasticity. It was then a natural consequence to consider hydrogen-related fracture as a type of brittle fracture and to include the function of hydrogen in the controlling process of the fracture, i.e., the thermodynamic instability of a crack as the critical stage. In the following, major brittle fracture models so far proposed are reviewed from mechanistic viewpoints. However, experimental difficulties, particularly in detecting hydrogen behaviors and revealing fine microstructural details, made early works on the function of hydrogen rather conceptual.

9.1 Internal Pressure Theory

Historically, internal cracks named "snowflakes", "fisheyes" or "white spots" are the earliest known hydrogen-induced defects in steel. Bright and shiny facets suggested high-pressure molecular hydrogen precipitation, and the precipitation sites were assumed to be "inter-block disjunctions" in crystals causing local cleavage and rupture [1]. The hydrogen source is mostly moisture in the atmosphere during the fabrication process of steel.

The hydrogen solubility in bcc iron in thermal equilibrium with hydrogen gas of pressure P follows Sieverts' law in Eq. (1.1). For iron, when hydrogen introduced under a hydrogen atmosphere of 0.1 MPa at 1273 K (1000 °C) is quenched to room temperature, the expected pressure of internally precipitated hydrogen gas is 4×10^6 MPa in equilibrium with the supersaturated lattice hydrogen concentration, enough to

M. Nagumo, *Fundamentals of Hydrogen Embrittlement*,
https://doi.org/10.1007/978-981-99-0992-6_9

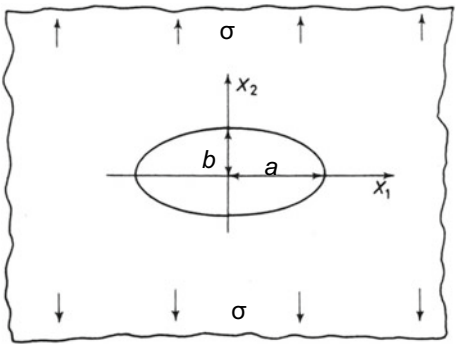

Fig. 9.1 Geometry of an elliptical hole in homogeneous linear elastic solid under applied tensile stress σ

cause cracking. Estimated hydrogen fugacity at various cathodic electrolysis methods is shown in Table 2.1.

(a) Griffith Condition

The internally pressurized crack can act as an incipient crack for brittle fracture. The basic notion of brittle fracture is the classical Griffith condition proposed for the fracture of glass. A model describes the thermodynamic instability of an elliptical hole in a homogeneous linear elastic solid under tensile stress, as illustrated in Fig. 9.1. The critical condition for unstable crack growth is that the release of the potential energy supplied by the internal strain and external force exceeds the increase in the surface energy. The expression for a crack of half-length a in a solid of surface energy γ and Young's modulus E in plane-strain condition is,

$$\sigma_f = \sqrt{2E\gamma/\pi(1-\upsilon^2)a}, \tag{9.1}$$

where σ_f is the fracture stress and υ is Poisson's ratio. The surface energy is defined as the energy to create a unit area of the new surface. The lower γ and the longer a decreases σ_f.

Tetelman and Robertson detected microcracks of 10^{-4} m in length on {100} planes of 3%Si-iron single crystals by hydrogen introduced under strong cathodic charging in 4% H_2SO_4 added with CS_2 and As_2O_3 at a current density of 160A/m^2 at room temperature [2]. Arrays of decorated dislocations were revealed, indicating intermittent growths of cracks associated with plastic deformation. The reasonable origin is a buildup of internal pressure by hydrogen and its decrease associated with the crack growth. Tetelman et al. replaced σ_f in Eq. (9.1) with the internal pressure P for a penny-shaped crack and calculated stress fields around the crack tip. The calculated results matched well the observed growth of the crack and slip traces. The deduced ratio of the energy expended in restarting the crack to the energy expended in moving it was of the order of unity for cracks 10^{-4} m long, implying a small contribution of plasticity that blunted the crack in this case. The internal pressure estimated from Eq. (9.1), neglecting the contribution of plasticity, was about 100 MPa.

(b) Incipient crack

The existence of an incipient crack is a crucial premise for brittle fracture. The void formation at non-metallic inclusions, like elongated MnS in particular, has been well-known concerning hydrogen-induced cracking (HIC) for line-pipe steel exposed to humid environments containing H_2S [3]. The molecular precipitation of hydrogen entering from environments forms voids.

On the other hand, some models for the plasticity-induced nanocrack formation for brittle fracture have been proposed as schematically shown in Fig. 9.2: (a) Stroh's model for the pileup of dislocation groups at the interface such as grain boundaries [4] and (b) Cottrell's model for coalescence of dislocations moving on intersecting slip planes [5]. In the former, the critical shear stress τ_c acting on pileup of n dislocations to coalesce into a crack is.

$$\tau_c = \tau_i + \left(\frac{12\gamma}{nb}\right), \tag{9.2}$$

where τ_i is the friction stress in the slip plane, γ is the surface energy, and b is the Burgers vector. The smaller n needs the larger τ_c to coalesce piled-up dislocations.

Cottrell pointed out the vital role of hydrostatic tension in the growth of a crack nucleus [5]. The instability of a microcrack under external stress, in addition to internal pressure, was given by Garofalo et al. [6] and Bilby et al. [7]. The basic idea is the same as the Griffith model, i.e., a crack's catastrophic growth occurs when the Gibbs free energy change is negative. For a wedge-shape crack produced by n dislocations running into the crack on a slip plane, the instability condition under an internal pressure p and applied external stresses, which produce a normal stress σ_1 and a shear stress σ_2, was given in the form,

$$\left[(\sigma_1 + p)^2 + \sigma_2^2\right]^{1/2} + [(\sigma_1 + p)\sin\theta - \sigma_2\cos\theta] \geq \frac{4\gamma}{nb}, \tag{9.3}$$

where θ is the angle between the crack and the slip plane, γ is the surface energy, and b is the Burgers vector of the dislocations [7]. The critical length $2c^*$ of the crack

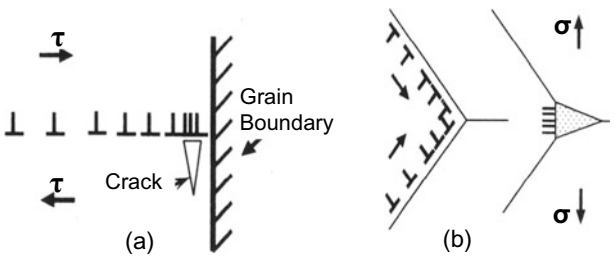

Fig. 9.2 Dislocation models for nanocrack formation. **(a)** Stroh's model for pileup of dislocations at interface such as grain boundaries. **(b)** Cottrell's model for coalescence of dislocations moving on intersecting slip planes

was

$$2c^* = 4\mu\gamma\{\pi(1-\nu)\varphi[\varphi + (\sigma_1 + p)\sin\theta - \sigma_2\cos\theta]\}^{-1}, \tag{9.4}$$

where μ and ν are the shear modulus and Poisson's ratio, respectively, and φ is defined as

$$\varphi^2 = (\sigma_1 + p)^2 + \sigma_2^2. \tag{9.5}$$

Another expression of $2c^*$ in terms of n is

$$2c^* = nb\mu[\pi(1-\nu)\varphi]^{-1}. \tag{9.6}$$

The magnitude of $2c^*$ in Eq. (9.4) was computed assuming hydrogen pressure corresponding to the lattice hydrogen concentration of 8 mass ppm and γ values that include an expected decrease due to hydrogen adsorption on the crack surface (described in Sect. 9.2). The calculated $2c^*$ for the observed fracture stress of mild steel at 158 K was about 6 or 4 nm, assuming γ of 0.83 or 0.52 J/m^2. The values are much shorter than observed 1 ~ 4 μm for hydrogen-free cases [6]. The assumed hydrogen concentration was under an unrealistically high p-value of 3100 MPa. Also, the assumed γ was much less than γ considering plastic deformation around the crack.

Usually, observed hydrogen is mainly trapped hydrogen rather than in solid solution, and nanoscale cracks predicted by the models in Fig. 9.2 have not been observed experimentally. Application of Stroh's model to actual brittle fracture has some other difficulties, such as the sharpness of the crack tip, the relaxation of high stresses on piled-up dislocations due to the activation of secondary slip systems, and complex microstructures particularly near grain boundaries in high-strength steel.

9.2 Surface Adsorption Theory

A decrease in the surface energy γ in the Griffith condition Eq. (9.1) promotes the instability of a crack. Lowering of γ of metals by hydrogen adsorption on the surface is given as Eq. (5.10) in Sect. 5.3.3 according to the Gibbs adsorption isotherm and the Langmuir adsorption. Petch assumed a crack ahead of arrays of n edge dislocations held up at some obstacle under a shear stress τ [8]. The Stroh model for the microcrack formation gives a relationship among τ, n, and γ in the form

$$\tau = 12\gamma/nb. \tag{9.7}$$

The dislocation arrays produce normal stress as a part of the fracture stress superposing the external stress. Also, assuming that the array length is one-half the grain diameter, Petch calculated γ as a function of the hydrogen concentration using

Eq. (5.10) and Sieverts' law that related the internal pressure to the hydrogen concentration. The results for α-iron at room temperature are shown in Fig. 5.8. The initial decrease in γ amounts to almost 90% by hydrogen concentrations less than 1 mass ppm.

The calculated decrease in γ at very low hydrogen concentrations amounts to ~ 2 J/m^2, about 40% of the true surface energy γ_0 of metals, but it is still a very small fraction of the effective surface energies for fracture of the order of kJ/m^2, estimated from fracture toughness data of steel. A decrease in γ due to the surface adsorption of hydrogen is viable, but its quantitative contribution to observed degradation is an issue, as described in Sect. 5.3.3. According to his surface energy theory, Petch explained the observed fracture stress of mild steel with different grain sizes [8]. However, the amount of hydrogen used for his estimation was as much as 10 mass ppm. The used cathodic electrolysis in 4% H_2SO_4 containing poison at a current density of 3200A/m^2 was very strong, surely producing extraneous defects by electrolysis.

Tromans calculated more precisely changes in γ of α-iron due to hydrogen adsorption using a suitable adsorption isotherm [9]. The calculated decrease in γ from the value in vacuum was 0.5 J/m^2 at 100 MPa hydrogen gas at 298 K. Tromans also showed effects of local stress on γ instead of internal pressure. Hydrostatic stress increased the activity of hydrogen, and the calculated decrease in γ by local hydrostatic stress of 1 GPa was 0.2 J/m^2.

The fracture surface in hydrogen embrittlement (HE) often exhibits a fine mixture of plastic shearing-off and cleavage-like fracture. As described in Sect. 6.2.2.1 on the crack growth rate in gaseous hydrogen environments, the model by Vehoff and Roth on the crack-tip opening assumed that the fractional hydrogen coverage of particular sites right at the tip of a stressed crack controls the crack propagation in HE [10].

9.3 Lattice Decohesion Theory

9.3.1 Stress-Controlled Criterion

The Griffith condition, Eq. (9.1), is a thermodynamic criterion for the onset of instability of a crack without referring to the microscopic processes of crack extension. In the mechanistic aspect, the break of atomic bonds is to occur for the crack extension, and the stress concentration at the crack tip must exceed the cohesive strength. This is the stress-controlled criterion of brittle fracture. The Griffith model assumed an elliptical hole of $2a$ in length and the radius of curvature of ρ. The mechanistic condition of the bond separation by the stress concentration at the hole edge is

$$\sigma_{\max} = \sigma_a\left(1 + 2\sqrt{\frac{a}{\rho}}\right) \approx 2\sigma_a\sqrt{\frac{a}{\rho}} > \sigma_{\text{th}} \approx \frac{E}{6}, \tag{9.8}$$

where σ_a is the applied stress and σ_{th} is the ideal strength of metal with Young's modulus E. The magnitude of $\sigma_{\max}$ is very high. A numerical estimation for $\sigma_a =$ 100 MPa, $2a = 10\,\mu$m, and $E = 300$ GPa requires a very sharp ρ of atomistic scale as small as 1.6×10^{-10} m, unfeasible in practical steel. Oriani and Josephic formulated a stress-controlled unstable crack advance criterion for HE [11]. The work to cut n atomic bonds per unit area is twice the true surface energy γ,

$$2\gamma = n \int_{z_0}^{\infty} F(z)dz, \tag{9.9}$$

where F(z) is the cohesive force, z is the interatomic distance, and z_0 is the stress-free equilibrium value of z.

A further difficulty in the criterion is that the bond separation is not a sufficient condition in unstable crack extension. In the above numerical assumptions, γ must be low enough, close to the true surface energy of metals ~ 2 J/m^2, to satisfy the thermodynamic Griffith condition. When plasticity is involved in the crack extension, the magnitude of γ substantially increases, and a larger γ requires a higher σ_f in Eq. (9.1). Troiano assumed the hydrogen-decreased cohesive strength for the delayed fracture of high-strength steel but thought the formation of fracture embryo due to activated dislocation arrays [12]. An involvement of plasticity in the creation of new surfaces remarkably increases the effective surface energy.

A critical condition for the start of a crack is that the concentrated stress at the crack tip exceeds the maximum cohesive force as expressed

$$k'\sigma(L/\rho)^{1/2} = nF_m(c'), \tag{9.10}$$

where σ is the applied tensile stress, L is the crack length, ρ is the crack-tip radius, n is the number of atoms per unit area of the crystallographic plane, F_{m}(c′) is the maximum cohesive force at a local hydrogen concentration c', and k' is a numerical parameter. The assumption that Oriani and Josephic made [11] was that F_{m} decreases in proportion to hydrogen concentration c,

$$F_m(c) = F_m^0 - \alpha c, \tag{9.11}$$

where $F_{\mathrm{m}}{}^0$ is F_{m} of the hydrogen-free lattice and α is an unknown parameter. The model was thus designated as the hydrogen-enhanced decohesion (HEDE) theory.

Estimating $F_{\mathrm{m}}(c)$ is difficult, but it is included in the stress intensity factor K, a parameter to express stress fields near the crack tip, described in the following Sect. 9.3.2. Using Eq. (9.10) for the stress-controlled brittle fracture, K is

$$K = k''\rho^{1/2}nF_m(c'), \tag{9.12}$$

where k'' is a numerical parameter. A buildup of c' by hydrostatic stress at the crack tip was considered in the calculation. Oriani et al. embedded $F_{\mathrm{m}}(c')$ in the critical stress

intensity K_{cr} for the onset of unstable fracture, using numerical $F_m(c')$ determined with experimental parameters. The local hydrogen concentration c is a function of the hydrostatic stress. Oriani et al. derived a relation between the environmental hydrogen gas pressure and K, using $F_m(c)$ and crack-tip radius as parameters. The ad hoc parameters were determined to fit the calculation using the formula with the experimental dependence of the critical hydrogen pressure on K.

The model was examined by experiments using WOL specimens of AISI 4340 steel in hydrogen and deuterium gases of pressures lower than 0.1 MPa at room temperature. Examples of thus determined parameters for K_{cr} of 20 ksi·in$^{1/2}$ (= 22 MPa·m$^{1/2}$) were the hydrostatic pressure of 2.49×10^3 ksi (= 17.4 GPa), the local hydrogen concentration of $6.75 \times 10^{-6}\beta$ (H/M), and $F_m(c)/{F_m}^0$ of 0.34. Experimental data Oriani et al. referred to were of intergranular (IG) fracture, and the unknown parameter β for the local hydrogen concentration was estimated to exceed 10^3 at grain boundaries. The fit between experimental and theoretical dependencies of p on K was good, but the estimated values of the hydrostatic stress and the local hydrogen concentration are not likely realistic.

Hydrogen effects on the crack-tip sharpness is a vital issue in HE of steel. A molecular dynamics (MD) simulation demonstrated a suppressed dislocation emission from the crack tip in iron by hydrogen, preventing blunting of the crack tip [13]. Two crack-tip geometries and orientations were considered, the crack plane normal of (111) [11$\bar{2}$] and (111)[1$\bar{1}$0] both orientations having a dislocation slip system available for easy dislocation emission. The system was initially deformed to a load $K_I = 0.8$ MPa m$^{1/2}$ that provided a driving force for hydrogen segregation toward the crack tip. Hydrogen atoms were then randomly inserted into interstitial sites within a cylindrical region of radius 10 nm around the crack tip. The fracture events at the crack tip were then investigated as a function of the applied load and the extent of hydrogen aggregation around the crack tip. Hydrogen atoms segregated to the crack surfaces started to aggregate in the vicinity of the loaded crack tip and formed a hydrogen-rich region. A local phase transformation from bcc to fcc structures occurred in the hydrogen-rich region. When the hydrogen concentration increased to 35 ~ 122/nm, the hydrogen-rich region blocked dislocation emission, and instead, with increasing applied load, brittle cleavage occurred. A crack-tip ductile-to-brittle transition induced by hydrogen aggregation was the main result of the study, but the hydrogen-rich zone was like a hydride.

9.3.2 Local Stress Intensity Approach

An alternative and general expression of the brittle fracture model is to use the stress intensity factor K. K expresses stress fields near the crack tip in the regime of linear elasticity as,

$$\sigma_{ij} = \frac{K}{\sqrt{2\pi r}} f(\theta) \tag{9.13}$$

in polar coordinates. Events that happen near the crack tip are controlled by K. For a through-crack of length $2a$ in an infinite plane at right angles to a uniform stress field σ, K is expressed as

$$K = \sigma\sqrt{\pi a}. \tag{9.14}$$

The critical value of K gives a failure criterion in a zone of a certain extent, but it per se does not specify the microscopic fracture process. K_{cr} is useful as a parameter to express the fracture toughness of materials for engineering purposes, but the viability of expressing stress fields in terms of K breaks down in regions very close to the crack tip and in the presence of local plasticity. As described in Sect. 9.4.2(a), the *immediate vicinity of the crack tip is crucial* for the crack extension. Some modifications have been proposed for such local situations. The fracture criterion Eq. (9.12) that uses the maximum cohesive force, Eq. (9.10), is for the case of the stress-controlled fracture. However, it is to be noticed that observed critical values of K for fracture *do not specify microscopic processes that cause the fracture event*.

Dislocations near the crack tip affect the crack-tip stress fields. When a crack is figured to occupy the negative real axis in the complex plane and dislocations are situated at points ζ_{j}, the stress at a point z is the superposition of the stresses exerted by the crack and the dislocations as expressed in the form,

$$\sigma = \frac{K}{\sqrt{2\pi z}} + \sum_j \frac{\mu\, b_j}{2\pi}\sqrt{\frac{\xi_j}{z}}\frac{1}{z-\varsigma_j}, \tag{9.15}$$

if, for simplicity, the distribution is symmetric about the x-axis [14]. The second term on the right-hand side is due to dislocations. By defining k_{D} and the local stress intensity factor k as.

$$k_D = \frac{\mu\, b}{\sqrt{2\pi\varsigma}}, \tag{9.16}$$

$$k = K - \sum_j k_D(j), \tag{9.17}$$

$\sigma(z)$ near the crack tip is expressed as [15]

$$\sigma(z) \approx \frac{k}{\sqrt{2\pi z}}. \tag{9.18}$$

Then, k is the effective stress intensity factor that determines the local stress fields in the presence of a dislocation group.

Marsh and Gerberich derived a relation between the plane-strain fracture toughness K_{IC} and the plane-strain Griffith local stress intensity for fracture k_{G} [16]. A simplified approximation was developed from computer simulations for the closest

approach of the nearest dislocation to the crack tip. The obtained relation is

$$K_{IC} \approx \frac{1}{\beta'} \exp\left(\frac{k_{IG}^2}{\alpha' \sigma_y}\right), \tag{9.19}$$

where α' and β' are parameters, and σ_y is the yield stress. Marsh and Gerberich assumed that the local hydrogen concentration C_H could proportionately lower k_{IG} to k_{IH} in the form

$$k_{IH} = k_{IG} - \alpha C_H. \tag{9.20}$$

An estimation of k_{IH} under hydrogen gas environments was to equate k_{IH} with $\sqrt{E\gamma}$, using about 1.5 ~ 1 J/m^2 for γ calculated according to Tromans' first-principles method [9]. The estimated k_{IH} replaced k_{IG}, and K_{IC} in the presence of hydrogen was calculated from Eq. (9.19). Using also separately determined parameters α' and β' in Eq. (9.19) to fit fracture toughness data of steel, the calculated threshold K decreased with increasing hydrogen gas pressures along a curve nearly coincident with observed data for AISI 4340 steel in hydrogen gas [11]. The fracture mode for the observed data was IG described in Sect. 7.2.4. The local stress intensity factor does not explicitly incorporate F_m, but Gerberich et al. ascribed the fit to the hydrogen-enhanced decohesion mechanism expressed by Eq. (9.12) [17].

9.4 Theories of Intergranular Fracture

9.4.1 Interface Decohesion

Enhanced embrittlement associated with the segregation of impurities in prior austenite grain boundaries is well-known concerning temper embrittlement of steel [18]. Enrichment of hydrogen along grain boundaries of steel has been revealed using tritium autoradiography [19, 20] and discussed concerning IG fracture [21]. Thermodynamics of the impurity adsorption at the interface affecting interfacial embrittlement has been presented in the literature [22–24].

The transition of a system from non-equilibrium to equilibrium states is associated with a net decrease in energy, as the Griffith condition expresses. Crack extension under an external force releases the internal strain energy U while the external force does work F. The driving force of the crack extension is the net change of the energy. The energy release rate or the crack driving force or the crack extension force, $\mathcal{G}$, is defined as

$$\mathcal{G} = -\frac{\mathrm{d}}{\mathrm{d}A}(U - F), \tag{9.21}$$

where A is the crack area.

The net change of the energy is transferred to the work to create new surfaces, W_s, and the equilibrium condition for the crack is

$$-\frac{\mathrm{d}}{\mathrm{d}A}(U - F) = \frac{\mathrm{d}W_s}{\mathrm{d}A}. \tag{9.22}$$

In the Griffith condition, the right-hand side of Eq. (9.22) is 2γ, and the surface energy term in the Griffith condition expresses the crack extension force. A general and extensive energy balance criterion for the crack extension was in a pioneering work by Rice [25]. When the separation of material surfaces incorporates microstructural processes associated with plasticity, the meaning of the right-hand side of Eq. (9.22) is not identical to the surface energy. Descriptions of Rice's model are at the end of Sect. 9.4.2(a).

Rice and Wang presented a fundamental idea for the crack advance *accompanying gradual interface decohesion*, schematically shown in Fig. 9.3 [23]. The crack extension force $\mathcal{G}$ along the transition zone of length ω between two elastic solids is defined as.

$$\mathcal{G} = \int_{\delta_0}^{\infty} \sigma(\delta) d\delta \equiv 2\gamma_{\mathrm{int}}, \tag{9.23}$$

where δ is the local interfacial opening. In this model, *the separation is reversible on stressing*, i.e., the separated faces rejoin when removed the applied stress. $2\gamma_{\mathrm{int}}$ in Eq. (9.23) is the thermodynamic threshold for growth *without including plastic work*.

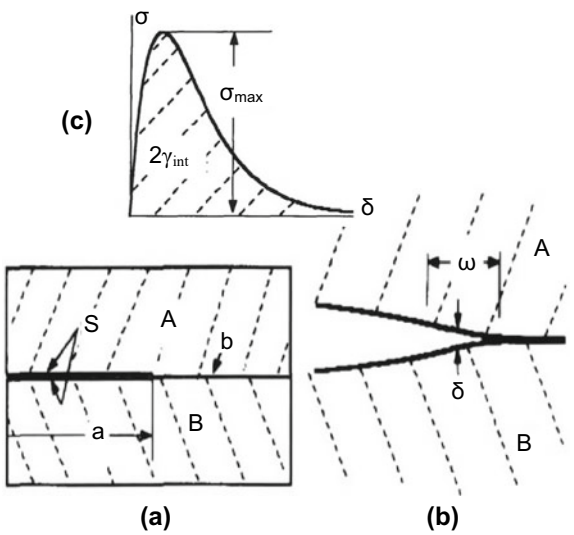

Fig. 9.3 Model of interface decohesion. **(a)** Interfacial brittle crack between phases A and B. **(b)** Region of gradual decohesion neat tip over a size scale ω. **(c)** Tensile stress σ versus separation distance δ normal to the interface (Rice et al. [23])

The impurity segregation at the interface increases the energy of the interface by the potential energies of segregants. The energy change du associated with the reversible change of a state is

$$du = Tds + \sigma d\delta + \sum_i \mu_i d\Gamma_i, \tag{9.24}$$

where T is temperature, s is entropy, and μ_i and Γ_i are, respectively, the equilibrium chemical potential and concentration of the i-segregant. Using Eqs. (9.23) and (9.24), Rice and Wang formulated the change in $2\gamma_{\text{int}}$ for the interface separation under a constant concentration or chemical potential of a segregant.

The segregation of impurities was assumed to follow the Langmuir-McLean theory that derived the fractional monolayer segregation to minimize the energy of the system,

$$\frac{\Gamma}{\Gamma^{\max} - \Gamma} = x \exp\left(-\frac{\Delta g}{RT}\right), \tag{9.25}$$

where x is the fraction of available sites in the bulk to be occupied by the segregant and Δg is the Gibbs free energy of segregation per mole of segregant. Rice and Wang derived an approximate form of $2\gamma_{\text{int}}$ for the case of fixed and low Γ in the form,

$$2\gamma_{\text{int}} = (2\gamma_{\text{int}})_0 - \left(\Delta g_b^0 - \Delta g_s^0\right)\Gamma, \tag{9.26}$$

where suffixes 0, b, and s abbreviate, respectively, segregant-free, boundary, and surface. Reported values of $(\Delta g_b{}^0 - \Delta g_s{}^o)$ for P, Sn, and Sb are in the range 50 ~ 100 kJ/mol. When one assumes that segregants occupy of one-quarter of possible adsorption sites, the second term of the right-hand side of Eq. (9.23) is 0.35 ~ 0.70 J/m^2, a substantial fraction of the true surface energy of metals.

Following Rice-Wang's theory, Novak et al. proposed a model that a dislocation pileup against a grain-boundary carbide which leads to interface decohesion and IG fracture, as an explanation of the role of hydrogen-enhanced plasticity in IG fracture [26]. Assumed hydrogen functions were in two ways: one was to reduce the reversible work for the decohesion along the carbide/matrix interface and the other was to enhance dislocation motion increasing the number of piled-up dislocations. Novak et al. applied the model to four-point bending tests of thermally hydrogen-charged AISI 4340 steel. Many assumptions and numerical estimations were made as listed below for quantitative analyses:

(1) In the second term on the right-hand side of Eq. (9.26), $(\Delta g_b{}^0 - \Delta g_s{}^o)$ of hydrogen was set to 74.5 kJ/mol, within the same range as that for P, Sn, and Sb.
(2) Trapped hydrogen in dislocations affects decohesion, rather than hydrogen strongly trapped in other sites such as grain or interface boundaries. The hydrogen occupancy for dislocations, $\theta_T^{(d)}$, was used in the interfacial coverage Γ,

$$\Gamma = \eta\, \theta_T^{(d)}\, \Gamma_{\max}, \tag{9.27}$$

with a fitting parameter η. The number of trap sites per unit area of the interface, $\Gamma_{\max}$, was determined from observed carbide size and frequency.

(3) The hydrogen concentration at the interface was estimated assuming transport by dislocations. The density of dislocations near the notch root was calculated using a finite element method.

(4) The weakest-link model was applied to estimate the fracture stress caused by the carbide/matrix interface decohesion.

(5) The effective surface energy, γ_{eff}, in the Griffith condition for the instability of the interface-crack, included plastic work γ_{p} accompanying the decohesion initiation event, in the form

$$\gamma_{\text{eff}} = 2\gamma_{\text{int}} + \gamma_{\text{p}}, \tag{9.28}$$

$$\gamma_{\text{p}} = A(2\gamma_{\text{int}})^q, \tag{9.29}$$

with parameters A and q.

The parameters were determined to fit calculated fracture stress with observed ones for various hydrogen concentrations. The second term on the right-hand side of Eq. (9.26) expresses the reduction in $2\gamma_{\text{int}}$ by hydrogen segregation. The expression of Γ is in Eq. (9.27), and the estimated value of Γ was 5×10^{-5} mol/m^2 ($= 3 \times 10^{-19}$/m^2) for the average hydrogen concentration of 1 at ppm. The calculation used assumed or calculated values [26], i.e., $\Delta g_b = -25.5$ kJ/mol, $\Delta g_s = -100$ kJ/mol, $\theta_T^{(d)} = 5 \times 10^{-4}$, $\eta = 0.01$, and $\Gamma_{\max} = 6.17 \times 10^{24}$ /m^2. The estimated reduction in $2\gamma_{\text{int}}$ by hydrogen was 3.8 J/m^2, which is about one order of magnitude larger than the values by the segregation of P and Sn, and almost completely cancels out the true surface energy of metals. The effective surface energy, considering the energy dissipation due to plasticity, was obtained from Eqs. (9.28) and (9.29). Taking $A = 0.02$ and $q = 6$, the estimated magnitude of γ_{p} was 82 J/m^2 for $2\gamma_{\text{int}}$ of 4 J/m^2. The crack extension force in Eq. (9.23) or $2\gamma_{\text{int}}$ in Fig. 9.3 is the essential quantity in the interface separation. Hydrogen effects on $2\gamma_{\text{int}}$ are included in the Gibbs free energy changes in Eq. (9.26), and the involvement of plasticity makes an estimation of $2\gamma_{\text{int}}$ complicated.

Instead, Yamaguchi et al. conducted first-principles calculations on grain-boundary embrittlement in metal-hydrogen systems [27], calculating the total segregation energy changes, $\Delta E_{\text{gb}}{}^{\text{seg}}$ and $\Delta E_{\text{s}}{}^{\text{seg}}$, when hydrogen atoms move from the bulk to grain boundary or free surface. Yamaguchi et al. defined $2\gamma_{\text{int}}$ as the difference between $2\gamma_{\text{S}}$ and γ_{GB}, as schematically shown in Fig. 9.4. The first-principles calculations by Yamaguchi et al. used the unit cell consisting of 76 Fe atoms and $\sum 3(111)$ symmetrical tilt grain boundaries in a bcc lattice. One hydrogen atom was

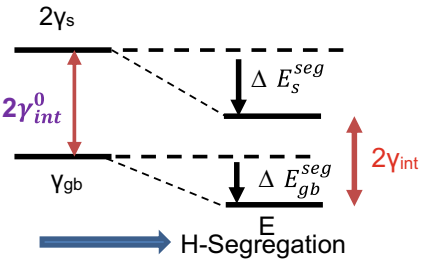

Fig. 9.4 Work for grain-boundary separation $2\gamma_{\text{int}}$ with and without hydrogen segregation (Yamaguchi et al. [27])

successively inserted at each interstitial site in the unit cell until the segregation energy reached a constant value. Calculated values of $\Delta E_{\text{gb}}{}^{\text{seg}}$ on FeΣ3(111) grain boundary and $\Delta E_{\text{s}}{}^{\text{seg}}$ on Fe(111) are − 45 and − 79 kJ/mol, respectively. The total segregation energy decreased with the hydrogen concentration, and the resultant decrease in $2\gamma_{\text{int}}$ was as much as 40% when six immobile hydrogen atoms were present in a unit cell area of 0.278 nm^2 on a FeΣ3(111) boundary.

Yamaguchi et al. also showed a more pronounced decrease in $2\gamma_{\text{int}}$ when hydrogen atoms were mobile, while the concentrations in the boundary and free surface in thermal equilibrium were the same as in bulk [28]. However, $2\gamma_{\text{int}}$ shown in Fig. 9.4 was the difference of the total energies before and after the interface separation. Their definition is not the crack extension force in Fig. 9.3(c). $2\gamma_{\text{int}}$ in Fig. 9.4 is the driving force for the interface separation, but the separation does not proceed spontaneously. Overcoming the energy barrier is also a necessary condition for fracture.

Kirchheim et al. applied the DEFACTANT mechanism described in Sect. 3.1.2 to the grain boundary or interface decohesion [29]. The reduction of the interfacial energy by impurity segregation is expressed by Eq. (9.3.11) in Sect. 3.1.2 in terms of the excess chemical potential of impurities.

$$\mathrm{d}\gamma = -\Gamma_A \mathrm{d}\mu_A. \tag{9.3.11}$$

However, a significant chemical potential or hydrogen pressure is requisite to cause a remarkable reduction of the work to fracture, defined as the difference between the newly created surface energy and the interface energy before separation. Quantitative estimations for an iron–hydrogen system predicted hydrogen pressure above 1GPa or hydrogen fugacity 10^8 bar to decrease the work to fracture. The vapor pressure of liquid water of about 20 mbar at room temperature gives about 20 MPa or 200 bar hydrogen fugacity in iron [29]. When dislocations or vacancies are present, enhancements of both the generation and movement rates by hydrogen are feasible.

9.4.2 Meaning of Surface Energy in Fracture Criteria

(a) Effective surface energy

A critical problem in applying the Griffith condition to IG fracture is the physical meaning of the surface energy γ. The effective surface energy "γ" derived from the observed fracture strength or K_{cr} using Eqs. (9.1) and (9.14) is of the order of 1 kJ/m^2, about three orders of magnitude higher than the true surface energy γ of metals. A common understanding of the difference is the involvement of plastic work γ_p in γ, as conventionally written as Eq. (9.28). However, the plastic processes that compose γ_p are difficult to figure for estimating γ_p.

McMahon and Vitek considered the work done by plastic deformation around the crack tip [30]. A model that McMahon and Vitek proposed was that the plastic region associated with the crack growth was a strip laid down along either side of the crack path. The plastic work W_p is proportional to the effective applied tensile stress σ_{eff} and plastic strain ε_p,

$$W_p \propto \sigma_{eff}\varepsilon_p V_p, \tag{9.30}$$

where V_p is the volume of the plastic region. McMahon and Vitek considered γ_p as the change of W_p at the crack extension, i.e.,

$$\gamma_p = \frac{dW_p}{da}. \tag{9.31}$$

The plastic strain rate $\dot{\varepsilon}_p$ associated with the crack extension is proportional to $\partial\varepsilon_p/\partial a$, and $\dot{\varepsilon}_p$ is empirically related to stress σ as,

$$\dot{\varepsilon}_p \propto \sigma_{eff}^m, \tag{9.32}$$

Since γ_p relates to $\dot{\varepsilon}_p$ according to Eqs. (9.30) and (9.31), γ_p also relates to σ_{eff}. Utilizing differentiation of logarithmic functions, the relation of γ_p with σ_{eff} is

$$\frac{d\gamma_p}{\gamma_p} \approx (m+1)\frac{d\sigma_{eff}}{\sigma_{eff}}. \tag{9.33}$$

McMahon and Vitek assumed two processes at the crack tip, one is bond stretching and rupture, and the other is dislocation emission and motion. A further assumption was that the two processes were independent and the crack extension was very fast, the bond stretching occurring only at the crack tip [30]. The purpose of the assumption was to separate the true surface energy γ from γ_p. The local stress at the crack tip dominates the bond breaking and is proportional to σ_{eff}. Since the true surface energy γ is the work done by the local stress, γ is proportional to σ_{eff}. Then, from Eq. (9.33), a relation between γ and γ_p was obtained in the form

$$\frac{d\gamma_p}{\gamma_p} \approx (m+1)\frac{d\gamma}{\gamma}. \tag{9.34}$$

The impurity segregation reduces the ideal surface energy γ, and the problem is whether the reduction in γ affects γ_p. That hydrogen reduces not only the reversible work but also the attendant plastic work was the implicit assumption of Eq. (9.29) that Novak et al. applied to decohesion of the carbide/matrix interface.

Alternatively, Jokl et al. considered a moving microcrack under stress and assumed concomitant bond breaking and dislocation emission from the crack tip [31]. In their model, the stress ahead of the crack and the microcrack opening displacement varied with time, and the plastic work γ_p was ascribed to the energy consumed by dislocation emission. Jokl et al. derived a thermodynamic criterion for the unstable microcrack extension taking into account the movement of newly created dislocations. Using the relationship between stress and dislocation velocity of the form of Eq. (9.32), γ_p was numerically computed as a function of the ideal work for fracture γ with several adjustable parameters. The calculated γ_p values were about 2 ~ 5 times as large as γ.

McMahon and Vitek's model could correlate a significant change in γ_p with a small change in γ. The crack-tip condition determines the instability of a crack, and Rice formulated under a thermodynamical scheme a general crack instability criterion incorporating plastic work [25]. Figure 9.5 shows his model [25]. In contrast with the Griffith model in Fig. 9.1, a cracked continuum is loaded by forces per unit area $\underline{T}$ on the portion of bounding surface A_t and per unit volume $\underline{F}$ throughout the region V occupied by the body. Displacements $\underline{U}$ are imposed on the portion of bounding surface A_U. No particular assumptions are made in the constitutive equations that relate stresses and strains. The crack extension increases the traction-free crack surface by an amount A'.

The energy balance criterion is that the work of applied forces during crack extension equals the change in stored elastic energy, dissipated energy, kinetic energy, and

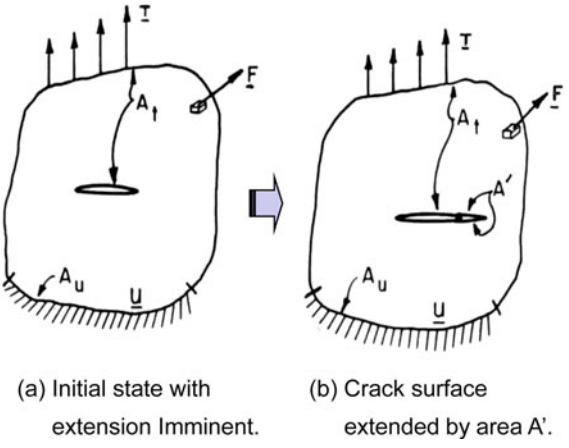

Fig. 9.5 Model of cracked continuum loaded by surface and body forces, imposed displacement on the portion of bounding surface. The crack extension increases the traction-free crack surface (Rice [25])

energy of the newly created surface. The last term is $\gamma A'$. The fracture criterion is then,

$$\lim \frac{1}{A'} \int_{V_0} \left\{ \int_{(a)}^{(b)} \left[\left(\sigma_{ij}^b - \sigma_{ij} \right) d\varepsilon_{ij} + \rho \left[\left(\ddot{u}_i^b - \ddot{u}_i \right) du_i \right] \right] \right\} dV = \gamma, \tag{9.35}$$

where V_0 denotes any arbitrary small region surrounding the crack tip and ρ is the mass density. Superscript a or b in Eq. (9.35) on any mechanical quantity denotes its value in the initial or extended states, respectively, in Fig. 9.5.

Rice calculated each term of the energy change with the configurations depicted in Fig. 9.5 for an infinitesimal crack extension. The derived fracture criterion states that the crack instability is determined *solely by singularities* in the stress and deformation fields at the crack tip, i.e., by the local stresses and deformations in the immediate vicinity of the crack tip. The *immediate vicinity* means an arbitrarily small portion that surrounds the crack tip and contains A′. The physical meaning of $\gamma A'$ is the work done by the new crack surfaces against forces tending to hold them together. The value of $\gamma A'$ is determined independently of the changes of elastic and dissipated energies, and *its estimation needs microstructural considerations* on processes separating material surfaces.

(b) Griffith condition for plasticity-induced crack at carbide

The presence of an incipient crack is a premise of energy balance criteria. Observed fracture toughness values include energies dissipated in forming the incipient crack, adding to energies needed for the crack instability. McMahon and Vitek considered the brittle crack nucleation at carbides in grain boundaries located a distance x from the precrack tip [30]. The crack was assumed to be formed by the pileup of dislocations at the carbide/boundary interface. Formerly, Smith formulated the Griffith condition for a crack produced by dislocation pileup at a carbide of 2c in length [32]. When the crack length along the interface between the carbide is c, and the dislocation pileup length is L, the Griffith condition for the crack, using Eq. (9.28) for γ_{eff}, was,

$$\sigma_L^2 + \tau_{\text{eff}}^2 \left[\left(\frac{L}{c} \right)^{1/2} + \frac{4}{\pi} \frac{\tau_{\text{f}}}{\tau_{\text{eff}}} \right]^2 \geq \frac{4E\left(2\gamma + \gamma_{\text{p}}\right)}{\pi\left(1 - \nu^2\right)c}, \tag{9.36}$$

where σ_{L} is the local stress ahead of the precrack, τ_{eff} is the effective shear stress on the dislocation pileup, E is Young's modulus, and ν is Poisson's ratio.

In this case, the local stress σ_{L} at the carbide in terms of the critical stress intensity K_C is

$$\sigma_L = \frac{K_{\text{C}}}{\sqrt{2\pi x_0}}, \tag{9.37}$$

where x_0 is the distance from the pre-crack tip to the point of microcrack nucleation. Equation (9.36) is the instability criterion for the newly created microcrack, but the magnitude of γ_p can be expressed in terms of the macroscopic fracture toughness K_{IC} or crack extension force $\mathcal{G}_{IC}$ that characterizes stress fields around the pre-crack under plane-strain condition. Using Eq. (9.36) and assuming $\tau_f \ll \tau_{eff}$ and $\gamma \ll \gamma_p$, $\mathcal{G}_{IC}$ is approximated as

$$\mathcal{G}_{IC} = \frac{K_{IC}^2(1-v^2)}{E} = 32\left(\frac{x_0}{L+4c}\right)\gamma_p, \tag{9.38}$$

If the magnitude of $x_0/(L+4c)$ were of the order of 10–10^2, $\mathcal{G}_{IC}$ would be 10^2–$10^3\gamma_p$. The multiplying factor of γ_p in Eq. (9.38) originates in stress fields that act on the dislocation pileup at carbides. McMahon and Vitek adopted the idea that related γ_p to dislocation dynamics as described concerning Eqs. (9.30) and (9.31) [30]. Then, it was deduced that a slight change in γ results in a significant change in the observed K_{IC} or $\mathcal{G}_{IC}$, according to the interrelation between γ and γ_p expressed by Eq. (9.29). Their model rationalized hydrogen-enhanced IG fracture caused by the reduction in γ due to enriched hydrogen in grain boundaries.

As described above, the involvement of plasticity in the instability criteria of cracks has been considered in various ways. A substantial part of observed fracture toughness is the plastic work dissipated prior to forming an incipient crack. The initiation site of brittle fracture is not the crack tip but generally in a region apart from the notch front associated with plasticity. The energy dissipated for incipient crack nucleation is substantial. Instrumented Charpy impact tests for medium-strength steel exhibited that the initiation of the brittle fracture determines the temperature dependence of the fracture toughness in the ductile-to-brittle transition temperature regions [33]. The energy dissipated preceding the onset of brittle fracture dominated the observed impact toughness values. The functions of hydrogen in fracture must be examined for the macroscopic crack initiation and growth stages and throughout the process that leads to the final fracture.

9.5 Summary of Brittle Fracture Models

The presence of an incipient crack and its instability are two critical issues in brittle fractures. For the former, the crack formation by the precipitation of molecular hydrogen is viable when hydrogen fugacity is high, but the function of hydrogen in triggering the unstable crack extension for the latter issue is a different problem. Cleavage fracture that characterizes the brittle fracture of bcc steel is scarcely observed in hydrogen embrittlement, and most models of hydrogen-related fracture of high-strength steel address intergranular (IG) fracture.

The classical Griffith condition for brittle fracture [34] stands on the thermodynamic energy balance criterion in extending a preexisting incipient crack. An alternative model is Rice-Wang's [23] gradual interface decohesion model as the transition between states of different surface energies. The latter model is general for the crack advance associated with little plasticity, not necessarily limited to catastrophic brittle fractures. The models do not specify the microscopic process of crack nucleation and extension while implicitly postulating the hydrogen function to reduce the cohesive strength of metallic atoms. Some ab initio calculations have shown a decrease in the cohesive force or the surface and interface energies by hydrogen under crucial assumptions of the hydrogen concentration and the incipient crack geometry.

On the other hand, some concepts developed in fracture mechanics, like crack extension force and process zone, are viable for the crack advance dominated by local plasticity other than atomic-bond decohesion. Experimentally, hydrogen effects are evaluated regarding the critical stress intensity factor or the crack extension force. The observed crack extension force derived from fracture toughness data is usually two or three orders of magnitude higher than the true surface energy of metals γ that represents the cohesive force. The discrepancy between the observed crack extension force and the true surface energy has been ascribed to plastic energy γ_{p} associated with a crack extension.

The entity of γ_{p} is a crucial issue, and some models proposed an interplay of γ with γ_{p}. Assuming the microcrack formation by the dislocation pileup at grain-boundary carbides, a numerically reasonable relation between a macroscopic crack extension force and γ_{p} was derived. However, it is to be noticed that observed fracture toughness values include *energies dissipated in the specimen until forming the incipient crack and its instability*, even in regions in the specimen not directly concerned with the critical event. Rice's generalized energy balance criterion [25] noticed that plasticity in the *immediate vicinity* of the crack tip solely determines the crack instability. The entity of γ_{p} that affects instability must be investigated regarding plasticity within this limited region.

Another problem of the stress-controlled fracture model for crack instability is that the crack tip must be atomically sharp. The reduced γ by hydrogen in the energy balance criteria implies the reduction in the cohesive strength that constitutes γ. However, the reduced cohesive strength is still very high, exceeding the yield stress of the material and causing blunting of the crack tip. The situation makes it difficult to keep the sharpness of the crack tip to satisfy stress-controlled instability criteria.

The hydrogen effect on the crack instability criteria through plasticity is a crucial issue. Apparently brittle appearance of fracture in HE does not rule out fracture processes dominated by mechanisms other than brittle bond breaking or interface separation. Accordingly, a rigorous definition of brittle fracture beyond macroscopic appearance is not certain. Plasticity-dominated fracture is not ruled out in some cases to which the local stress intensity approach or the interface decohesion model has been applied. Microscopic information was limited in early sophisticated studies, but recent advances in experimental and theoretical tools are revealing microscopic entities, helping understand the function of hydrogen in cacking, as presented in the preceding chapters.

References

1. C.A. Zapffe, J. Member, C.E. Sims, Trans. AIME **145**, 225–263 (1941)
2. A.S. Tetelman, W.D. Robertson, Acta Metall. **11**, 415–426 (1963)
3. A. Ikeda, Tetsu-to-Hagané **70**, 792–802 (1984)
4. A.N. Stroh, Proc. Roy. Soc. London A **232**, 548–560 (1955)
5. A.H. Cottrell, Trans. Metall. Soc. AIME **212**, 192–203 (1958)
6. F. Garofalo, Y.T. Chou, V. Ambegaokar, Acta Metall. **8**, 504–512 (1960)
7. B.A. Bilby, J. Hewitt, Acta Metall. **10**, 587–600 (1962)
8. N.J. Petch, Phil. Mag. **1**, 331–337 (1956)
9. D. Tromans, Acta Metall. Mater. **42**, 2043–2049 (1994)
10. H. Vehoff, W. Rothe, Acta Metall. **31**, 1781–1793 (1983)
11. R.A. Oriani, P.H. Josephic, Acta Metall. **22**, 1065–1074 (1974)
12. A.R. Troiano, Trans. ASM **52**, 54–80 (1960)
13. J. Song, W.A. Curtin, Nat. Mater. **12**, 145–151 (2013)
14. R.M. Thomson, J.E. Sinclair, Acta Metall. **30**, 1325–1334 (1982)
15. I.-H. Lin, R. Thomson, Acta Metall. **34**, 187–206 (1986)
16. P.G. Marsh, W.W. Gerberich, Acta Metall. Mater. **42**, 613–619 (1994)
17. W.W. Gerberich, P.G. Marsh, J.W. Hoehn, in *Hydrogen Effects in Materials*, ed. by A.W. Thompson, N.R. Moody (TMS, Warrendale, 1966), pp. 539–551.
18. R.A. Mulford, C.J. McMahon Jr., D.P. Pope, H.C. Feng, Metall. Trans. A **7A**, 1184–1195 (1976)
19. M. Aoki, H. Saito, M. Mori, Y. Ishida, M. Nagumo, J. Jpn. Inst. Metals **58**, 1141–1148 (1995)
20. T. Asaoka, C. Dagbert, M. Aucouturier, J. Galland, Scr. Metall. **11**, 467–472 (1977)
21. C.J. McMahon Jr., Eng. Fract. Mech. **68**, 773–788 (2001)
22. J.P. Hirth, J.R. Rice, Metall. Trans. A **11A**, 1501–1511 (1980)
23. J.R. Rice, J.-S Wang, Mater. Sci. Eng. **A107**, 23–40 (1989**)**
24. Y. Misin, P. Sofronis, J.L. Bassani, Acta Mater. **50**, 3609–3622 (2002)
25. J.R. Rice, in *Proceedings of International Conference on Fracture* vol.1 (The Japan Society Promotion of Science, 1965), pp. A269–A318.
26. P. Novak, R. Yuan, B.P. Somerday, P. Sofronis, R.O. Ritchie, J. Mech. Phys. Solids **58**, 206–226 (2010)
27. M. Yamaguchi, K. Ebihara, M. Itakura, T. Kadoyoshi, T. Suzudo, H. Kaburaki, Metall. Mater. Trans. A **42A**, 330–339 (2011)
28. M. Yamaguchi, J. Kameda, K. Ebihara, M. Itakura, H. Kaburaki, Phil. Mag. **92**, 1349–1368 (2012)
29. R. Kirchheim, B. Somerday, P. Sofronis, Acta Mater. **99**, 87–98 (2015)
30. C.A. McMahon Jr., V. Vitek, Acta Metall. **27**, 507–513 (1979)
31. M.L. Jokl, V. Vitek, C.J. McMahon Jr., Acta Metall. **28**, 1479–1488 (1980)
32. E. Smith, in *Proceedings of Conference Physical Bases of Yield and Fracture* (Institue of Physics, Physics Society, Oxford, 1966), pp. 36–46
33. T. Tani, M. Nagumo, Metall. Mater. Trans. A **26A**, 391–399 (1995)
34. A.A. Griffith, Trans. Royal Soc. London, A-221 (1920)